CORE
Metadata, citation and similar papers at core.ac.uk
Provided by University of Strathclyde Institutional Repository

Dogrul, Ali and Ozdemır, Yavuz Hakan and Sezen, Savas and Barlas, Barıs (2018) Uncertainty assessment and self-propulsion estimation of Duisburg Test Case. In: 3rd International Symposium on Naval Architecture and Maritime, 2018-04-23 - 2018-04-25, Yildiz Technical University. ,

This version is available at https://strathprints.strath.ac.uk/67912/

Strathprints is designed to allow users to access the research output of the University of Strathclyde. Unless otherwise explicitly stated on the manuscript, Copyright © and Moral Rights for the papers on this site are retained by the individual authors and/or other copyright owners. Please check the manuscript for details of any other licences that may have been applied. You may not engage in further distribution of the material for any profitmaking activities or any commercial gain. You may freely distribute both the url (https://strathprints.strath.ac.uk/) and the content of this paper for research or private study, educational, or not-for-profit purposes without prior permission or charge.

Any correspondence concerning this service should be sent to the Strathprints administrator: strathprints@strath.ac.uk

The Strathprints institutional repository (https://strathprints.strath.ac.uk) is a digital archive of University of Strathclyde research outputs. It has been developed to disseminate open access research outputs, expose data about those outputs, and enable the management and persistent access to Strathclyde's intellectual output.

Uncertainty Assessment and Self-Propulsion Estimation of Duisburg Test Case

Ali Dogrul*, Yavuz Hakan Ozdemir, Savas Sezen*, Baris Barlas*****

***Yildiz Technical University, Istanbul, Turkey**, adogrul@yildiz.edu.tr, sezen@yildiz.edu.tr

****Canakkale 18 Mart University, Canakkale, Turkey**, yhozdemir@comu.edu.tr

***** Istanbul Technical University, Istanbul, Turkey**, barlas@itu.edu.tr

Abstract

In this study, hydrodynamic performance of Duisburg Test Case (DTC), a Post-Panamax container vessel, has been investigated by using Computational Fluid Dynamics (CFD) tools. Total resistance analyses have first been performed using an optimum grid number which has been determined by verification and validation processes based on Grid Convergence Index (GCI). Later, open water propeller analyses have been carried out by applying GCI for uncertainty approach. Finally, self-propulsion analysis has been made for DTC hull by modelling the propeller using body force method for design speed. The major outcome of this study is to emphasize on the uncertainty assessment for calculating the ship's total resistance and its open water propeller analyses. Additionally, the feasibility of body force method on self-propulsion performance prediction is discussed.

Keywords: Body Force Method, Computational Fluid Dynamics, Duisburg Test Case, Grid Convergence Index, Propeller-Hull Interaction, RANSE, Uncertainty

1. Introduction

Propeller-hull interaction has been an important issue in recent years. Several methods have been used to determine this interaction. Model experiments and numerical methods have been widely used for this purpose. Different CFD methods such as potential theory and finite volume method have been applied to model propeller-hull interaction. This interaction can be simulated by modeling the propeller itself or modeling an actuator disc based on body force method.

Several researches have been made about estimating the self-propulsion performance of marine vessels. In the study of Moctar et al. (2012), hydrodynamic performance of DTC hull has been investigated by performing model experiments of total resistance, open water propeller and self-propulsion. Berger et al. (2011) have investigated the self-propulsion performance of the well-known benchmark case KRISO

container ship (KCS) by using both potential flow solver and a RANS solver. A hybrid URANS-LES model has been applied to compute the unsteady loadings on a marine propeller behind the KVLCC2 tanker model by Abbas et al. (2015). The numerical results have been compared with different empirical estimations. Zhang (2010) has also investigated self-propulsion of KCS numerically. The viscous flow around KCS hull has been investigated with an operating propeller by applying body force and sliding mesh approaches. The results of these approaches have been compared with the experimental one. It is seen that CFD method is feasible for prediction of propeller-hull interaction. Bugalski and Szantyr (2014) have investigated the unsteady propeller performance by using a developed lifting surface code. The numerical analyses have been performed for five different cases including the original hull and hull with four different wake improvement devices. Rijpkema et al. (2013) have studied the propeller-hull interaction by simulating the steady viscous flow around KCS hull with RANS method and unsteady propeller flow with BEM. The coupled RANS-BEM approach has given accurate results for thrust compared with the experimental data. Visonneau et al. (2012) have validated their in-house developed CFD code by investigating the viscous flow around KCS hull with the presence of the propeller (INSEAN E779A). The interaction between hull and propeller has been analyzed with CFD and the results have been compared with the experiments. The developed CFD code has shown a promising performance. The research of Win et al. (2013) is focused on the interaction between Series 60 hull and a 5 bladed fixed pitch propeller using a CFD code coupled with a quasi-steady blade element theory. The analyses have been carried out with and without propeller and both results have been compared with the available experimental data. Stern et al. (1994) have made a study for validation of a viscous flow method solving the flow around a propeller in the presence of a hull. The study investigates the effect of the turbulence model (k-ϵ) and the grid density on the harmonics of the propeller performance parameters both in steady and unsteady manner. The numerical results have been compared with the ones of an inviscid method.

Zhang and Zhang (2014) have examined the interaction between a propeller and a submarine hull numerically. The analyses have been made by taking the free surface effect into account. The results show a good agreement with the experiments. It is highlighted that the free surface is more important than self-propulsion on total resistance. A seven bladed INSEAN E1619 propeller has been studied in the presence of DARPA Suboff submarine model by Chase and Carrica (2013). The numerical analyses have been made by employing Delayed Detached Eddy Simulation (DDES) approach. A comprehensive study about self-propulsion of submarine has been done by Sezen et al. (2018). Self-propulsion characteristics of DARPA Suboff bare hull and appended hull have been estimated using two methods: body force method and modeling the actual propeller. It is concluded that the numerical method is sufficient for self-propulsion prediction of underwater vehicles.

In this study, open water propeller flow computations and the total resistance calculations of DTC hull are predicted by solving RANS equations. First, the numerical method has been verified in terms of

open water propeller flow and ship free surface flow using GCI technique by means of grid number. The numerical method has then been validated with the available experimental data. Then, the open water propeller performance characteristics have been coupled with RANS simulations in order to estimate the self-propulsion point of DTC hull in design Froude number. The self-propulsion performance has been analyzed using Body Force Method (BFM).

2. Theoretical Background

2.1. Mathematical Formulation

The governing equations are the continuity and the RANS equations for the unsteady, three-dimensional, incompressible flow.

$$\frac{\partial U_i}{\partial x_i} = 0 \tag{1}$$

is the continuity,

$$\frac{\partial U_i}{\partial t} + \frac{\partial \left(U_i U_j \right)}{\partial x_j} = -\frac{1}{\rho}\frac{\partial P}{\partial x_i} + \frac{\partial}{\partial x_j}\left[\nu \left(\frac{\partial U_i}{\partial x_j} + \frac{\partial U_j}{\partial x_i} \right) \right] - \frac{\partial \overline{u_i' u_j'}}{\partial x_j} \tag{2}$$

is the momentum equations, where U_i is the mean velocity, u_i' is the fluctuation velocity components in the directions of the Cartesian coordinates x_i. P is the mean pressure, ρ is the density and ν is the kinematic viscosity of the fluid. The well-known k-ε turbulence model is used to simulate the turbulent flow around the hull. When there are no high pressure changes along the hull and no separation around the flow, k-ε turbulence model is a practical and useful tool for the turbulent closure. During the analyses, Reynolds stress tensor is calculated as follow;

$$\overline{u_i' u_j'} = -\nu_t \left(\frac{\partial U_i}{\partial x_j} + \frac{\partial U_j}{\partial x_i} \right) + \frac{2}{3}\delta_{ij} k \tag{3}$$

where, ν_t is the eddy viscosity and expressed as $\nu_t = C_\mu k^2 / \varepsilon$ while C_μ is an empirical constant. k is the turbulent kinetic energy and ε is the turbulent dissipation rate.

Further explanations for the k-ε turbulence model can be found in Wilcox (2006).

2.2. Uncertainty Assessment

In this study, uncertainty assessment has been carried out via Grid Convergence Index (GCI) as recommended in the ITTC procedure for CFD verification (2011a). This method firstly was proposed by Roache (1998) and then improved with different other studies. The procedure implemented in this study has been briefly explained in the following:

Let h_1, h_2 and h_3 are grid lengths and $h_1 < h_2 < h_3$. The refinement factors are as follows:

$$r_{21} = \frac{h_2}{h_1} \qquad r_{32} = \frac{h_3}{h_2} \tag{4}$$

Refinement factors should be greater than 1.3 in accordance with the experiments (Celik et al., 2008). Grid lengths' refinement has been selected as $\sqrt{2}$ given in the studies of Tezdogan et al. (2015) and Ozdemir et al. (2016). Because of the mesh algorithm, grid number has been used during the calculation of the refinement factors. This choice is crucial in uncertainty analyses especially for unstructured mesh system. Therefore, these values have been differentiated as:

$$r_{21} = \left(\frac{N_1}{N_2} \right)^{1/3} \qquad r_{32} = \left(\frac{N_2}{N_3} \right)^{1/3} \tag{5}$$

Difference between generated grid numbers can be calculated as below:

$$\varepsilon_{21} = X_2 - X_1 \qquad \varepsilon_{32} = X_3 - X_2 \tag{6}$$

At this point, convergence condition R can be examined as,

$$R = \frac{\varepsilon_{21}}{\varepsilon_{32}} \tag{7}$$

The solution has an oscillating convergence if -1<R<0, while the solution is monotonically convergent if 0<R<1 as stated in Stern et al. (2006).

3. Numerical Method

3.1. Geometry and Boundary Conditions

DTC Post-Panamax container ship model is a benchmark form. The main particulars of DTC ship are shown in Table 1. Figure 1 represents the 3-D model of DTC hull. For propeller analyses, the propeller of DTC hull has been used and the main particulars of the propeller are given in Table 2. 3-D model of the propeller is depicted in Figure 2.

Table 1. Main particulars of DTC hull

	DTC Model	DTC
λ	1/59.407	1
L_{pp} (m)	5.976	355.0
B_{wl} (m)	0.859	51.0
T (m)	0.244	14.5
∇ (m^3)	0.827	173467.0
C_B	0.661	0.661
WSA (m^2)	6.243	22032.0

Fig. 1. 3-D view of DTC hull

Table 2. Main particulars of DTC propeller

	Model Propeller	Propeller
λ	1/59.407	1
D (m)	0.150	8.911
P/D (0.7R)	0.959	0.959
A_E/A_0	0.800	0.800
c (0.7R) (mm)	0.054	3.208
D_h/D	0.176	0.176
Z	5	5
Rotation	Right	Right

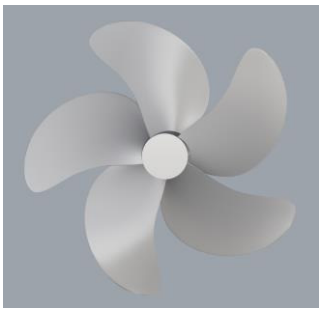

Fig. 2. 3-D view of DTC propeller

The computational domain has been selected to be adequate in dimensions to simulate the ship flow properly for resistance and self-propulsion analyses, which is identical to the recommended dimensions of ITTC guideline (2011b). Figure 3 shows the main dimensions of the computational domain and the boundary conditions applied on the surfaces.

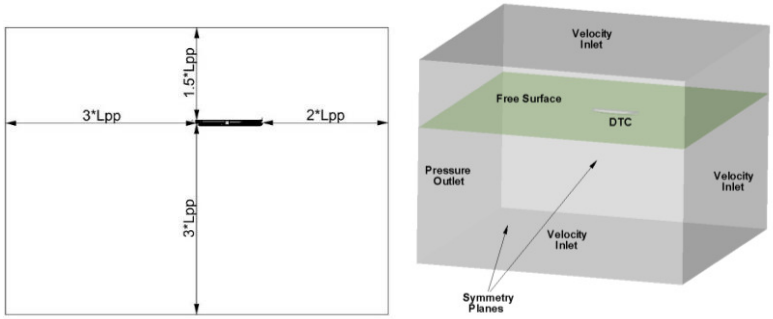

Fig. 3. Computational domain and boundary conditions for DTC hull

In order to conduct proper CFD analyses, the initial and boundary conditions should be defined carefully depending on the flow problem. Correct boundary conditions lead the simulations to accurate results and prevent unnecessary computational costs. Also the boundary conditions should be chosen wisely to ensure that they have no influence on the numerical solution (Date and Turnock, 1999). The right, top and bottom surfaces of the computational domain are defined as velocity inlet and the left side is defined as pressure outlet (Figure 3). The ship boundary is taken as no slip wall, which indicates that all the velocity components are zero on the hull surface. In addition, the lateral surfaces are defined as symmetrical ones in order to establish a numerical towing tank. More detailed information on boundary conditions can be found in the theory guide of the commercial CFD software STAR-CCM+ (2015).

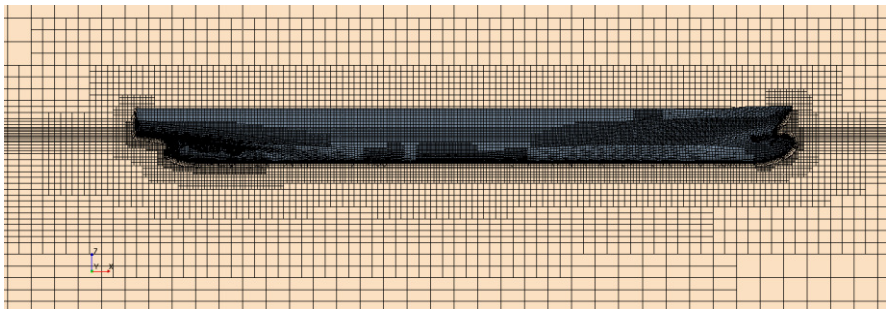

Fig. 4. Unstructured mesh around DTC hull

The computational domain is discretized by three dimensional finite volumes in compliance with FVM. For resistance analyses, proper mesh structure has been created around the ship hull using hexahedral elements. In order to create the control volume, trimmer meshing is employed. The trimmer meshing algorithm provides a fully hexahedral mesh structure avoiding the tetrahedral elements. The

computational domain is represented by hexahedral elements while finer elements are employed on the ship surface. A finer mesh is also employed near the stern region in order to well capture the wake region behind the ship. A mesh refinement is accomplished in the bow region to capture the turbulent flow characteristics in detail. Also local mesh refinements have been employed near the free surface for capturing the interaction between two phases (air and water) precisely. Unstructured mesh around the ship is given in Figure 4. Mesh size of the hull surface and the growth rate is adjusted in order to keep wall y^+ values in an acceptable range between 30 and 300.

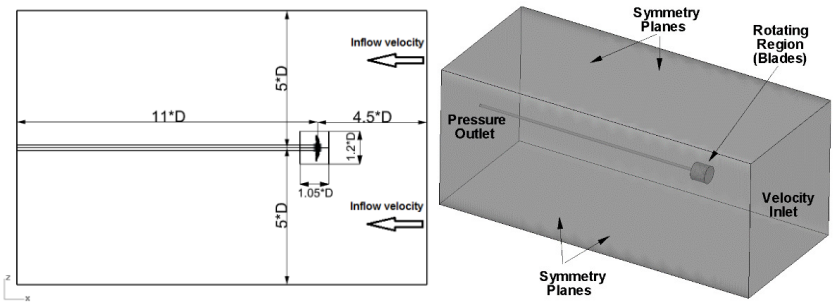

Fig. 5. Computational domain and boundary conditions for DTC propeller

Figure 5 shows the computational domain with the assigned boundary conditions on the surfaces of propeller working in open water condition. The left side of the computational domain is defined as pressure outlet while the right side is to be velocity inlet. The propeller blades and the shaft are considered as no slip wall that indicates all the velocity components on these surfaces are zero. The surrounding surfaces are defined as symmetry planes.

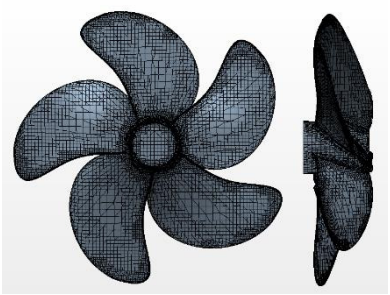

Fig. 6. Unstructured mesh on the propeller blades

For open water propeller analyses; hexahedral mesh structure has been employed using trimmer mesh algorithm. Also a mesh refinement has been embedded around the propeller disc in order to model the interaction of the hull and the propeller more accurately. Figure 6 shows the unstructured mesh applied on the DTC model propeller blades in open water analyses.

3.2. Solution Strategy

k-ε turbulence model is implemented in the numerical analyses which has been extensively used for industrial applications. The k–ε turbulence model has also been used accurately in many other studies performed in the same area, such as Tezdogan et al. (2015), Ozdemir et al. (2016). The pressure field is solved by using SIMPLE algorithm which is based on pressure-velocity coupling. All governing equations are discretized using a cell based FVM and the advection terms are discretized with a first-order upwind interpolation scheme.

Because of the flow characteristics, the analyses have been made by considering the free surface effects in resistance analyses. The flow field has been modelled including air and water phases. Viscous effects near the ship hull are taken into account by modelling the boundary layer with an appropriate grid structure keeping non-dimensional y^+ wall distance values of the hull in a reasonable range between 30 and 300 (Barlas, 2000). Rotational flow have been modeled using Moving Reference Frame (MRF) technique for open water propeller analyses. By this technique, the governing equations are transformed into a rotating frame to get a steady-state solution (Moussa, 2014). For self-propulsion analysis, an actuator disc has been modeled using body force method. Distribution of body forces has been applied in this actuator disc region. Here, actuator disc region represents an infinite number of blades of propeller. The hydrodynamic performance characteristics of model propeller have been defined in this region. The actuator disc and the model propeller have the same diameter and identical distributions of elemental thrust along the radius (Krasilnikov, 2013).

4. Verification and Validation

Three different grid sizes have been used for resistance and open water propeller analyses. The number of grids are given in Table 3. The resistance analyses have been conducted for DTC ship in model scale, while the open water analyses have been conducted for model propeller. According to Wilson et al. (2001), the foremost source of uncertainty of numerical results is because of the mesh system. Different grid numbers have been used for modelling the computational domain for resistance and propulsion analyses. For medium and fine grids, the difference between computation and the experimental results are less than 3.30% but the required time for reaching the converged solution is 10 hours longer in fine grid. It is concluded that using medium grids are good enough to predict the resistance and all simulations including total resistance, open water and self-propulsion with actuator disc were performed with medium grids.

Table 3. Number of grids for uncertainty analyses

	Resistance analysis	Open water propeller analysis
Grid type	Grid number	Grid number
Fine	1,434,396	1,897,822
Medium	820,578	1,147,883
Coarse	547,226	931,684

The free stream velocity has been considered as 1.335 m/s for total resistance of DTC during the uncertainty analyses. Convergence condition (R) is calculated as -0.524 for DTC that means the solution has an oscillating convergence. Advance coefficient (J) is taken as 0.5 in open water propeller analyses and R is calculated as 0.609 that means the solution is converging monotonically. Detailed information about Grid Convergence Index (GCI) can be found in Roache (1998). Table 4 presents the values of grid uncertainty for resistance and open water analyses.

Table 4. Uncertainty values for resistance and propulsion analyses

	Resistance analysis	Open water propeller analysis
Analysis set	% GCI_{FINE}	% GCI_{FINE}
1 2 3	1.22	0.43

The comparison of the numerical results with the experimental data is given in Table 5. The numerical results given are for the medium grid size. The uncertainty analyses for resistance calculations have been made while it has been carried out for open water test for non-dimensional thrust coefficient.

Table 5. Comparison of the numerical and experimental results for validation

	CFD	Experiment	Relative Difference (%)
R_T (N)	19.67	20.34	3.30
K_T	0.2697	0.276	2.28

5. Results and Discussions

Total resistance and resistance components of DTC bare hull model have been calculated with unsteady RANS approach. Open water propeller analyses have been conducted with model propeller. The open water performance of the model propeller has been defined in an actuator disc using body force method to obtain the self-propulsion point of DTC bare hull in design Froude number.

5.1. Resistance Analyses

The total resistance and resistance components of DTC bare hull model have been estimated using URANS based CFD method. The numerical analyses have been performed using the optimum grid size which is determined with verification and validation study. The time step size has been chosen as recommended in ITTC procedure (2011b). The numerical results have been compared with the available experimental data in terms of total resistance and other components (Moctar et al., 2012).

The numerical results are in a good agreement with the experimental data for total resistance as given in Figure 7. Also the friction resistance coefficient has been calculated similar with ITTC formulation (1957) as given in Figure 8. The wave resistance of the model ship has been calculated using the form factor (1+k=1.094) described in the study of Moctar et al. (2012). The numerical computations show a deviation in wave resistance coefficient when compared with the experimental data. The deviation increases with the increase in Froude number.

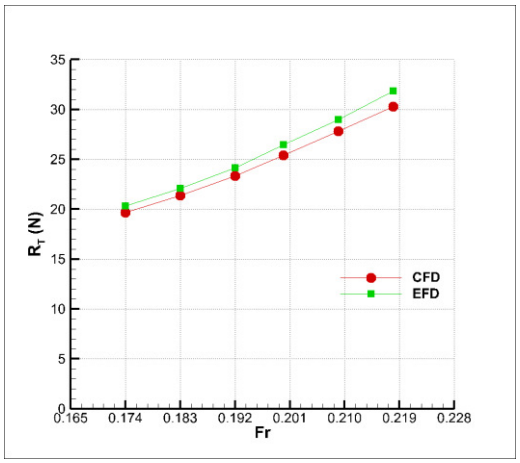

Fig. 7. Comparison of total resistance for DTC bare hull

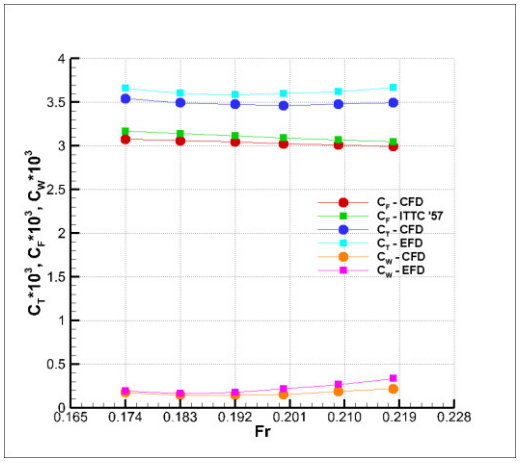

Fig. 8. Comparison of resistance components for DTC bare hull

Figure 9 shows the contour plot of free surface elevations around DTC hull at Fr=0.218. One can see the Kelvin wave system around the hull easily.

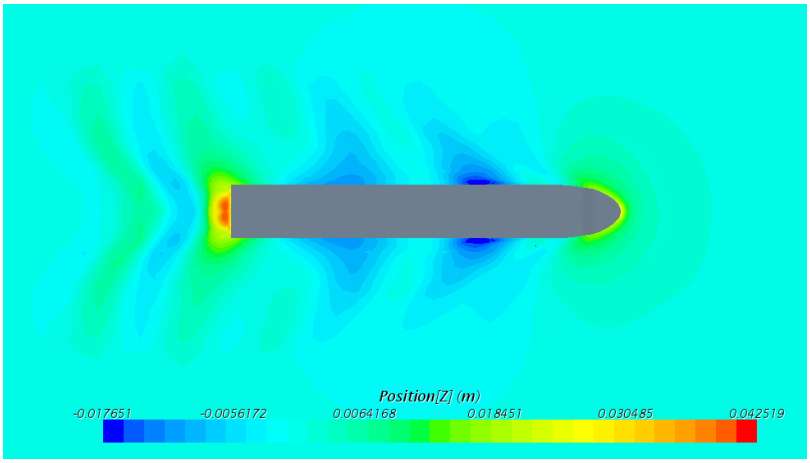

Fig. 9. Free surface deformation around DTC hull at Fr=0.218

5.2. Open Water Propeller Analyses

The open water propeller analyses have been performed with the model propeller of DTC to obtain the hydrodynamic performance characteristics at different advance ratios. The numerical analyses have been conducted using the optimum grid obtained from the verification and validation study. The results show that the numerical method predicts the hydrodynamic performance well when compared with the experimental data (Moctar et al., 2012). As depicted in Figure 10, the difference between the numerical simulations and the experiments increases in high advance ratios (J>0.6).

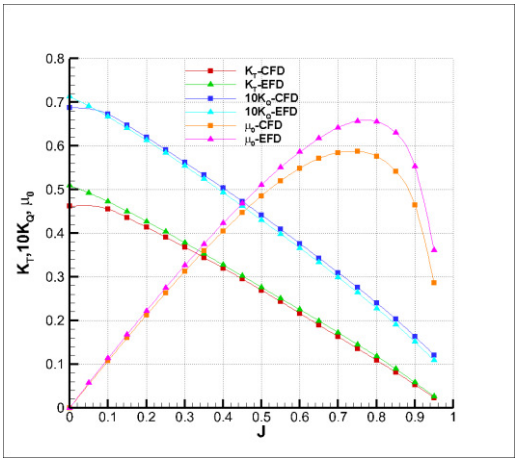

Fig. 10. Comparison of open water characteristics for DTC propeller

5.3. Self-Propulsion Analysis with Body Force Method

The self-propulsion analysis has been performed for DTC hull at design Froude number (Fr=0.218). The numerical model consists of the ship model and an actuator disc located in the propeller disc area instead

of modeling the actual propeller behind the hull. Hydrodynamic performance characteristics of the model propeller have been defined in the actuator disc in order to represent the model propeller behind the hull. The self-propulsion point has been estimated as the propeller rotation speed which produces enough thrust force to overcome the total resistance of bare hull in self-propelled case. Figure 11 shows the free surface deformation around DTC hull at Fr=0.218 for self-propulsion case. Because of the rotating flow behind the hull, there is an asymmetry in the free surface deformation behind the hull. The free surface deformation behind the hull in transverse direction for bare hull and self-propulsion cases can be seen in Figure 12. The actuator disc causes a slight difference in the transversal free surface deformation behind the hull.

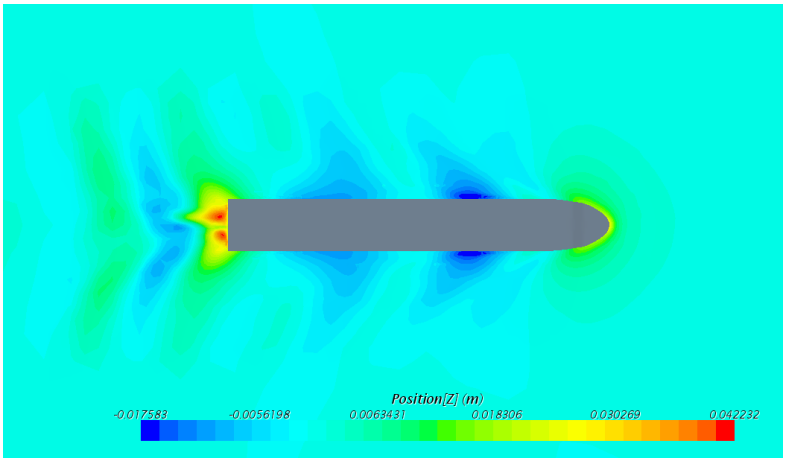

Fig. 11. Free surface deformation around DTC hull at Fr=0.218 with body force method

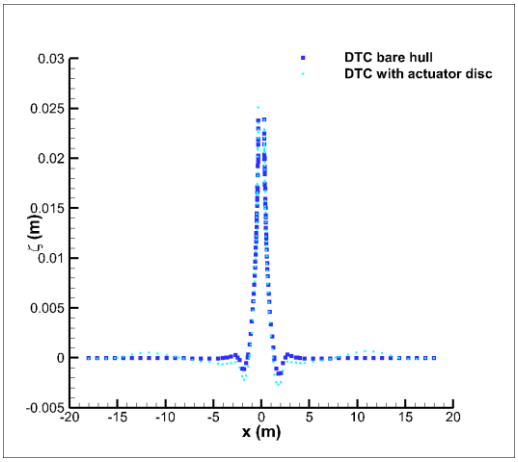

Fig. 12. Free surface deformation of bare hull and hull with actuator disc at x=-0.5 m distance at Fr=0.218

After determining the self-propulsion point of DTC hull, self-propulsion characteristics of DTC has been found using the following equations.

$$t = 1 - \frac{R_T}{T} \tag{8}$$

$$F_{D_M} = \frac{1}{2}\rho_M S_M V_M{}^2 \left(C_{T_M} - C_T\right) \tag{9}$$

Thrust deduction factor is represented by t while F_{D_M} denotes the friction deduction between model and full scale. Table 6 shows the self-propulsion characteristics of DTC hull with model propeller using body force method. The numerical results have been compared with the experimental self-propulsion results of Moctar et al. (2012). Since the self-propulsion point in the experiments is not given, no comparison has been made for self-propulsion point.

Table 6. Comparison of self-propulsion characteristics

	V_M (m/s)	n (rps)	t	F_{DM} (N)
CFD	1.668	16.5	0.193	16.520
Experiment	1.668	-	0.090	13.947

6. Conclusions

This study focuses on the estimation of self-propulsion point of DTC hull using an actuator disc based on body force method. Before simulating the self-propulsion point, total resistance and open water propeller analyses have been conducted. In order to determine the uncertainty of the numerical method, Grid Convergence Index (GCI) method has been employed. Verification and validation study has determined the optimum grid number. This grid has been used for the rest of the analyses. The self-propulsion point has been predicted numerically for design Froude number without modeling the propeller itself behind the hull. The open water propeller characteristics have been defined in an actuator disc located in the propeller disc area. The numerical result has then been used to calculate the thrust deduction factor of DTC model. It is concluded that the actuator disc may not be sufficient to be used for simulating the propeller-hull interaction for the ships moving in free surface because of the deviation in thrust deduction factor. For the future work, it is planned to focus on modeling the actual propeller behind the hull for observation of propeller-hull interaction.

References

Abbas, N., Kornev, N., Shevchuk, I., and Anschau, P. (2015). "CFD prediction of unsteady forces on marine propellers caused by the wake non-uniformity and non-stationarity," Ocean Eng., 104, 659–672. doi:10.1016/j.oceaneng.2015.06.007

Barlas, B. (2000). "Ship preliminary design and computational fluid dynamics," J. Turk. Nav. Acad.,.

Berger, S., Druckenbrod, M., Greve, M., Abdel-Maksoud, M., and Greitsch, L. (2011). "An Efficient Method for the Investigation of Propeller Hull Interaction," 14th Numerical Towing Tank Symposium.

Bugalski, T., and Szantyr, J. A. (2014). "Numerical Analysis of the Unsteady Propeller Performance in the Ship Wake Modified By Different Wake Improvement Devices," Pol. Marit. Res., 21, 32–39. doi:10.2478/pomr-2014-0027

Celik, I. B., Ghia, U., and Roache, P. J. (2008). "Procedure for estimation and reporting of uncertainty due to discretization in CFD applications," J. Fluids Eng.-Trans. ASME, , doi: 10.1115/1.2960953. doi:10.1115/1.2960953

Chase, N., and Carrica, P. M. (2013). "Submarine propeller computations and application to self-propulsion of DARPA Suboff," Ocean Eng., 60, 68–80. doi:10.1016/j.oceaneng.2012.12.029

Date, J. C., and Turnock, S. R. (1999). A study into the techniques needed to accurately predict skin friction *using RANS solvers with validation against Froude's historical* flat plate experimental data, Available: http://eprints.soton.ac.uk/46061/, (date last viewed: 28-Aug-15).

ITTC (1957). "Report of Resistance Committee," Proceedings of 8th ITTC, Madrid.

ITTC (2011). "75-03-01-04 CFD, General CFD Verification," ITTC - Recomm. Proced. Guidel.,.

ITTC (2011). "Practical guidelines for ship CFD applications," Proceedings of 26th ITTC, Hague.

Krasilnikov, V. (2013). "Self-Propulsion RANS Computations with a Single-Screw Container Ship," Third International Symposium on Marine Propulsors, Tasmania, Australia.

Moctar, O. el, Shigunov, V., and Zorn, T. (2012). "Duisburg Test Case: Post-Panamax Container Ship for Benchmarking," Ship Technol. Res., 59, 50–64. doi:10.1179/str.2012.59.3.004

Moussa, K. (2014). Computational Modeling of Propeller Noise: NASA SR-7A Propeller (MSc Thesis), University of Waterloo, Waterloo, Ontario, Canada.

Ozdemir, Y. H., Cosgun, T., Dogrul, A., and Barlas, B. (2016). "A numerical application to predict the resistance and wave pattern of KRISO container ship," Brodogradnja, 67, 47–65.

Rijpkema, D., Starke, B., and Bosschers, J. (2013). "Numerical simulation of propeller-hull interaction and determination of the effective wake field using a hybrid RANS-BEM approach," Third International Symposium on Marine Propulsor, Launceston, Tasmania, Australia. s.

Roache, P. J. (1998). "Verification of Codes and Calculations," AIAA J., 36, 696–702. doi:10.2514/2.457

Sezen, S., Dogrul, A., Delen, C., and Bal, S. (2018). "Investigation of self-propulsion of DARPA Suboff by RANS method," Ocean Eng., 150, 258–271.

"STAR-CCM+ Documentation," (2015).

Stern, F., Kim, H. T., Zhang, D. H., Toda, Y., Kerwin, J., and Jessup, S. (1994). "Computation of Viscous Flow Around Propeller-Body Configurations: Series 60 CB=06 Ship Model," J. Ship Res., 38, 137–157.

Stern, F., Wilson, R., and Shao, J. (2006). "Quantitative V&V of CFD simulations and certification of CFD codes," Int. J. Numer. Methods Fluids, 50, 1335–1355. doi:10.1002/fld.1090

Tezdogan, T., Demirel, Y. K., Kellett, P., Khorasanchi, M., Incecik, A., and Turan, O. (2015). "Full-scale unsteady RANS CFD simulations of ship behaviour and performance in head seas due to slow steaming," Ocean Eng., 97, 186–206. doi:10.1016/j.oceaneng.2015.01.011

Visonneau, M., Queutey, P., Deng, G. B., Guilmineau, E., Leroyer, A., and Mallol, B. (2012). "Computation of Free-Surface Viscous Flows around Self-propelled Ships with the Help of Sliding Grids," 11th International Conference on Computer Applications and Information Technology in the Maritime Industries.

Wilcox, D. C. (2006). Turbulence Modeling for CFD, D C W Industries, La Cãnada, Calif., 3rd edition.

Wilson, R. V., Stern, F., Coleman, H. W., and Paterson, E. G. (2001). "Comprehensive Approach to Verification and Validation of CFD Simulations—Part 2: Application for Rans Simulation of a Cargo/Container Ship," J. Fluids Eng., 123, 803–810. doi:10.1115/1.1412236

Win, Y. N., Tokgoz, E., Wu, P. C., Stern, F., and Toda, Y. (2013). "Computation of Propeller-Hull Interaction using Simple Body-Force Distribution Model around Series 60 CB = 06," J. Jpn. Assoc. Nav. Archit. Ocean Eng., 18, 17–27.

Zhang, N., and Zhang, S. (2014). "Numerical simulation of hull/propeller interaction of submarine in submergence and near surface conditions," J. Hydrodyn. Ser B, 26, 50–56. doi:10.1016/S1001-6058(14)60006-8

Zhang, Z. (2010). "Verification and validation for RANS simulation of KCS container ship without/with propeller," J. Hydrodyn. Ser B, 22, 932–939. doi:10.1016/S1001-6058(10)60055-8

View publication stats